



ELSEVIER

Contents lists available at ScienceDirect

Journal of Theoretical Biology

journal homepage: www.elsevier.com/locate/yjtbi

Numerical cell model investigating cellular carbon fluxes in *Emiliana huxleyi*



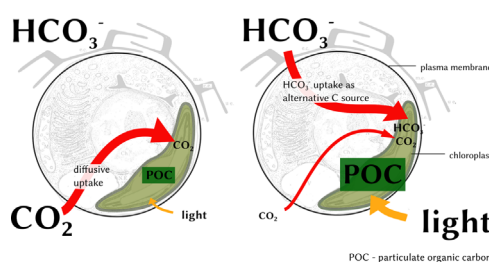
Lena-Maria Holtz*, Dieter Wolf-Gladrow, Silke Thoms

Alfred-Wegener-Institut, Helmholtz-Zentrum für Polar- und Meeresforschung, Am Handelshafen 12, 27570 Bremerhaven, Germany

HIGHLIGHTS

- Cellular C fluxes through coccolithophores are poorly understood.
- By means of a numerical cell model, we investigate cellular C fluxes through *Emiliana huxleyi*.
- In the model, CO₂ and HCO₃⁻ rarely inter-convert within the cytosol.
- At high external [CO₂] and low light, photosynthetic C demand can be covered by diffusive CO₂ uptake.
- CO₂ accumulation around RubisCO is possible without transporting C species uphill.

GRAPHICAL ABSTRACT



ARTICLE INFO

Article history:

Received 10 June 2014

Received in revised form

7 August 2014

Accepted 11 August 2014

Available online 16 September 2014

Keywords:

CO₂/carbon uptake

CCM

Coccolithophores

Fractionation

Phytoplankton

ABSTRACT

Coccolithophores play a crucial role in the marine carbon cycle and thus it is interesting to know how they will respond to climate change. After several decades of research the interplay between intracellular processes and the marine carbonate system is still not well understood. On the basis of experimental findings given in literature, a numerical cell model is developed that describes inorganic carbon fluxes between seawater and the intracellular sites of calcite precipitation and photosynthetic carbon fixation. The implemented cell model consists of four compartments, for each of which the carbonate system is resolved individually. The four compartments are connected to each other via H⁺, CO₂, and HCO₃⁻ fluxes across the compartment-confining membranes. For CO₂ accumulation around RubisCO, an energy-efficient carbon concentrating mechanism is proposed that relies on diffusive CO₂ uptake. At low external CO₂ concentrations and high light intensities, CO₂ diffusion does not suffice to cover the carbon demand of photosynthesis and an additional uptake of external HCO₃⁻ becomes essential. The model is constrained by data of *Emiliana huxleyi*, the numerically most abundant coccolithophore species in the present-day ocean.

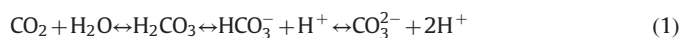
© 2014 The Authors. Published by Elsevier Ltd. This is an open access article under the CC BY-NC-ND license

(<http://creativecommons.org/licenses/by-nc-nd/3.0/>).

1. Introduction

Human activity has rapidly increased atmospheric carbon dioxide partial pressure (pCO₂) from about 280 μatm in year 1750 to around 400 μatm in 2013 (NOAA, 2013). A continuing strong increase is expected. Carbon dioxide (CO₂) dissolves in seawater and becomes part of the ocean's carbonate system, whose simplified

representation is:



Due to the inter-conversion between individual inorganic carbon species (iCS) and the high total alkalinity of seawater, the ocean exhibits a strong capacity to buffer anthropogenic CO₂ emissions. The uptake of CO₂, however, impacts the ocean's carbonate chemistry with potentially tremendous consequences for marine organisms and whole ecosystems. In this study, we focus on coccolithophores, unicellular calcareous algae that belong to the main pelagic calcifiers.

* Corresponding author. Tel.: +49 471 4831 2093.

E-mail address: lenna-maria.holtz@awi.de (L.-M. Holtz).

Nomenclature

Abbreviations used in text

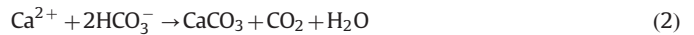
Ω	Calcite saturation product
CA	Carbonic anhydrase
CCM	CO ₂ /carbon concentrating mechanism
CV	Calcification/coccolith vesicle
DIC	Dissolved inorganic carbon, i.e. sum of CO ₂ , H ₂ CO ₃ , HCO ₃ ⁻ , and CO ₃ ²⁻
HC	High carbon

HL	High light
iCS	Inorganic carbon species, here CO ₂ , HCO ₃ ⁻ , or CO ₃ ²⁻
LC	Low carbon
LL	Low light
MIMS	Membrane inlet mass spectrometry
pCO ₂	CO ₂ partial pressure
PIC	Particulate inorganic carbon, here calcite
POC	Particulate organic carbon
RubisCO	Ribulose-1,5-bisphosphate-Carboxylase-Oxygenase

Most notably, coccolithophores impact the ocean's carbon cycle via the formation of particulate organic and inorganic carbon (POC and PIC). Our model organism *Emiliania huxleyi* is the most abundant and one of the best studied coccolithophore species.

During photosynthesis, POC is built from CO₂ inside the chloroplast. Particulate inorganic carbon is precipitated in the form of calcium carbonate (CaCO₃) from carbonate ions (CO₃²⁻) inside a specialised cell compartment termed calcification or coccolith vesicle (CV). Since internal pH homeostasis and charge neutrality have to be ensured (Wolf-Gladrow et al., 2007), the production of one mole POC either relies on one mole external CO₂ or one mole of bicarbonate ions (HCO₃⁻) plus one mole of protons (H⁺) (cf. Fig. 1). Correspondingly, the production of one mole PIC (i.e. CaCO₃) relies on one mole Ca²⁺ plus either one mole external HCO₃⁻ and the extrusion of one mole H⁺ or one mole CO₂ and the extrusion of two moles H⁺. The productions of POC and PIC thus impact the marine carbonate system differently: Particulate organic carbon production, i.e. CO₂ consumption, reduces the DIC (dissolved inorganic carbon) concentration in seawater and shifts the carbonate system towards higher pH values. Particulate inorganic carbon production, i.e. CO₃²⁻ consumption, decreases DIC and alkalinity in the molar ratio 1:2 and shifts the carbonate system towards lower pH values. In view of bulk seawater, it does not make a difference whether carbon for POC and PIC production is taken up in the form of CO₂ or HCO₃⁻. The composition of the external (seawater) carbonate system, however, impacts uptake rates of external iCS into the cell and therewith the fixation rates of internal iCS into POC and PIC. Intracellular pathways and conversion rates of iCS cannot be measured directly and are thus not known. Therewith, it is difficult to understand the interdependency between the marine carbonate system and POC and PIC production rates mechanistically.

In order to reveal the influence of abiotic conditions on the PIC: POC ratio of coccolithophores in a systematic manner, intracellular pathways of iCS have to be elucidated first. As mentioned above, it is not possible to measure intracellular iCS fluxes such as the CO₂ flux across the chloroplast envelope directly and *in vivo*. We hence rely on indirect information about these fluxes. External carbon sources of POC and PIC production have been an issue of discussion since more than five decades. Paasche (1964) demonstrated by means of short-term ¹⁴C incubations that external HCO₃⁻ is the main substrate for calcite production in *E. huxleyi*. The bulk of experimental work that was conducted afterwards has led to the same conclusion (Berry et al., 2002; Rost et al., 2002). For *E. huxleyi*, Paasche (1964) suggested that CO₂ intracellularly produced in the reaction



might be used in photosynthesis. Reaction (2) thus presumes external HCO₃⁻ being the carbon source for both, photosynthesis and calcite precipitation, and gives the sum of reactions (3) to (5) or (3), (4), (6), and (7) (cf. Zeebe and Wolf-Gladrow, 2001).

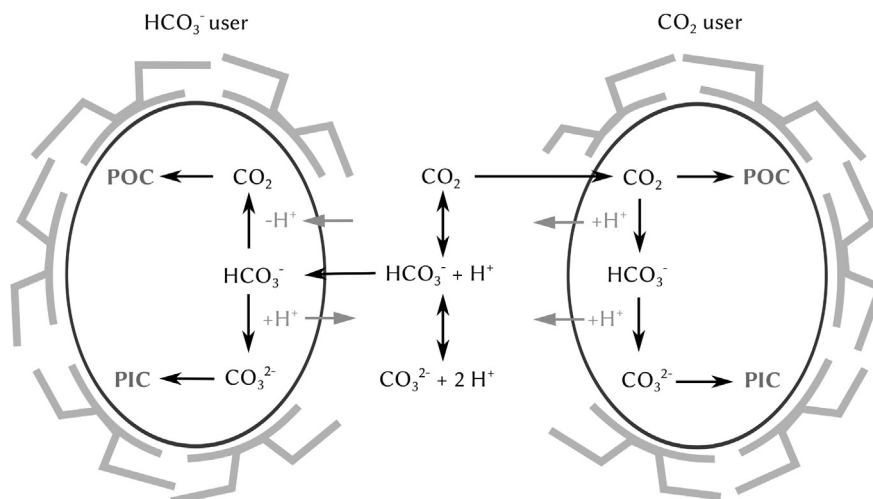
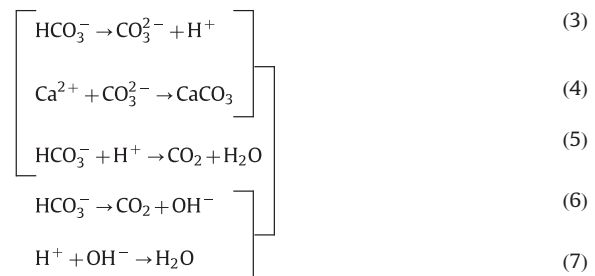


Fig. 1. Theoretical H⁺ budget related to the intracellular conversion of inorganic carbon species for a HCO₃⁻ using cell (left) and a CO₂ using cell (right). Photosynthesis and calcite precipitation are the two major processes that require dissolved inorganic carbon. PIC - particulate inorganic carbon, POC - particulate organic carbon.

In comparison to the other three reactions, reactions (5) and (6) are slow Reaction (5) can be accelerated by the enzyme carbonic anhydrase (CA) and is favoured under low pH values. Reactions (3), (4), (6), and (7) occur under high pH values and may hence constitute prominent reactions inside the CV. The stoichiometry, however, that is implied by reaction (2), i.e. release of one mole CO_2 per mole precipitated CaCO_3 , is unlikely to occur, primarily because the reaction rate of reaction (3) exceeds the one of reaction (6) by more than five orders of magnitude (at temperature 15°C and salinity 30). Nevertheless, the H^+ released during calcite precipitation (eqns. (3) and (4)) could contribute to CO_2 formation for photosynthetic use in another compartment (eqn. (5)). The relative strength of this coupling process would on the one hand depend on the sum of intracellular H^+ fluxes and on the other hand on the external carbon source for photosynthesis. In the same work, Paasche (1964) showed that external HCO_3^- as well as external CO_2 are used for photosynthesis. Later on, many experiments were conducted aiming to determine the external carbon source for photosynthesis. They partly lead to contradicting results (for an overview until year 2001 see Paasche, 2002). Rost et al. (2002) concluded from the distribution of stable carbon isotopes in POC that CO_2 as well as HCO_3^- are used for photosynthesis. Based on measurements of ^{14}C fluxes in disequilibrium, Rokitta and Rost (2012) identified external HCO_3^- as the major iCS source that supports POC production. The ^{14}C disequilibrium assay they used, however, was conducted at a higher pH value than the cells were acclimated to. Kottmeier et al. refined this ^{14}C disequilibrium assay, which enabled them to measure the external iCS source of POC at different assay pH values. They found external CO_2 being the major source for photosynthesis under current CO_2 conditions.

To sum up, it seems that external CO_2 and HCO_3^- are the carbon sources for POC production and external HCO_3^- is the only carbon source for PIC production which suggests that conversion of CO_2 to HCO_3^- inside the cytosol is low.

On basis of current knowledge about membrane transporters and enzymes in coccolithophores as well as in phytoplankton and plant cells in general, a numerical cell model is developed to investigate the pathways of inorganic carbon from the external medium towards the sites of calcite precipitation and photosynthesis. The model is used to examine the following three questions:

1. Can CO_2 and HCO_3^- pass the cytosol without being inter-converted?
2. Can enough external CO_2 be taken up by diffusion to satisfy the carbon requirement of POC production?

3. Can CO_2 be accumulated around RubisCO without inorganic carbon species being transported against concentration gradients?

2. Cell model

The cell is divided into four compartments: The cytosol, the CV, the chloroplast stroma, and the thylakoid/pyrenoid complex (Fig. 2). Our working hypothesis concerning the carbon concentrating mechanism (CCM), i.e. the mechanism that leads to CO_2 accumulation around RubisCO, is illustrated in Figure 3. Membrane- and compartment-specific characteristics assumed for the model's set-up are briefly described in the following. In Section 2.1, the mathematical implementation is described.

Plasma membrane. Aquaporins inside the plasma membrane facilitate diffusive CO_2 uptake (1 in Fig. 2). We use the permeability coefficient for CO_2 diffusion through the plasma membrane of *Nicotiana tabacum* which contains aquaporins (Uehlein et al., 2008). Protons pass the plasma membrane through voltage-gated H^+ channels in coccolithophores (passive direction: out of the cell) (Taylor et al., 2011). In the model, cytosolic pH (ca. 7; Anning et al., 1996) is regulated by means of these channels (3 in Fig. 2). Anion exchangers that are associated with HCO_3^- fluxes (assuming across the plasma membrane) were found in *E. huxleyi* (Herfort et al., 2002; von Dassow et al., 2009; Mackinder et al., 2011; Taylor et al., 2011; Rokitta and Rost, 2012; Bach et al., 2013). In our model, external HCO_3^- enters the cytosol following its concentration gradient (2 in Fig. 2) and thus cannot accumulate inside the cytosol. *In vivo*, HCO_3^- probably enters the cytosol in sym- or antiport with or against other ions. One possibility is a cotransport with Na^+ that may be energised by the electrochemical gradient driving Na^+ into the cell: The inner face of the plasma membrane is charged negatively and the external concentration of Na^+ furthermore exceeds the one inside the cytosol. As the internal Na^+ level has to remain low, Na^+ would subsequently have to be exported (potentially in antiport against H^+) at the expense of energy equivalents.

Coccolith vesicle membrane. We assume that CO_2 diffuses across the CV membrane directly, i.e. not through aquaporins (4 in Fig. 2), and use the CO_2 permeability coefficient measured for membranes of pure liposomes (Prasad et al., 1998). In the model, energy requiring $\text{Ca}^{2+}/\text{HCO}_3^-/\text{H}^+$ transporters (5 in Fig. 2, cf. Holtz et al., 2013) import the substrates for calcite precipitation against their concentration gradients and support the establishment of an

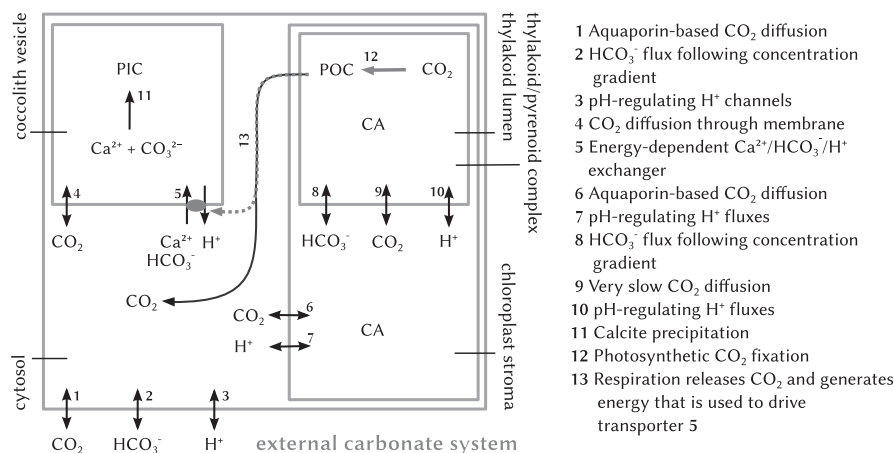


Fig. 2. Cell model including four compartments. Fluxes are indicated by arrows. Grey coloured arrows indicate rates that are set to a predefined value. The external carbonate system which forces cellular in- and efflux rates is set to the values measured by Rokitta and Rost (2012). CA - carbonic anhydrase; PIC - particulate inorganic carbon; POC - particulate organic carbon.

alkaline milieu that is favourable for calcite precipitation. These transporters are not known from literature. The assumed stoichiometry of $1 \text{ Ca}^{2+} : 1 \text{ HCO}_3^- : 1 \text{ H}^+$, however, ensures charge balance and also sufficiently high calcite saturation states (Ω) (cf. Wolf-Gladrow et al., 2007; Holtz et al., 2013). Calcite precipitation can take place at $\Omega > 1$ and it increases with increasing Ω values (11 in Fig. 2).

Chloroplast envelope and stroma. The chloroplast of coccolithophores is surrounded by four membranes, one of which does not constitute a significant barrier for CO_2 diffusion because it includes large pores. The implemented chloroplast stroma is thus surrounded by three membranes only which are taken into consideration via a CO_2 permeability coefficient that is three times lower than the one of a single membrane layer (cf. Thoms et al., 2001). We assume that all three membranes contain aquaporins to facilitate diffusive influx of CO_2 into the chloroplast (6 in Fig. 2). The existence of aquaporins in the chloroplast envelope has been shown for *N. tabacum* (Uehlein et al., 2008). The pH of the *in silico* chloroplast stroma (ca. 8) can be regulated via proton fluxes across the chloroplast envelope (7 in Fig. 2). Following the findings of Quiroga and González (1993) for coccolithophore CCMP-299, we assume CA activity inside the chloroplast stroma (outside the pyrenoid).

Thylakoid membrane and lumen. We assume that HCO_3^- , H^+ , and CO_2 fluxes connect the thylakoid lumen to the chloroplast stroma (8, 9, and 10 in Fig. 2). *In vivo*, HCO_3^- could enter the thylakoid through channels driven by the HCO_3^- concentration gradient and the positive charging of the thylakoids' inner face (due to high internal $[\text{H}^+]$). The influence of HCO_3^- channels on passive HCO_3^- fluxes from the chloroplast stroma into the thylakoid lumen was positively tested by means of a numerical model (Thoms et al., 2001) that takes into account the electrical potential difference across the thylakoid membrane. The electrochemical

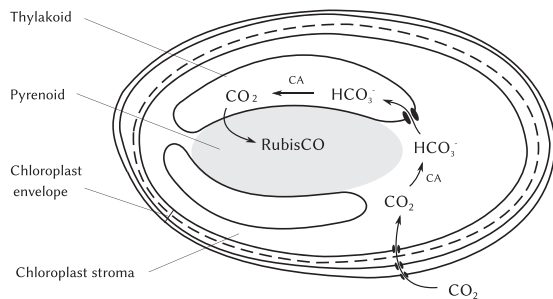


Fig. 3. Hypothetical chloroplast-based CCM for *Emiliana huxleyi*. Working hypothesis (similar to Pronina and Semenenko, 1992; Pronina and Borodin, 1993; Raven, 1997): Carbon dioxide enters the chloroplast from the cytosol via aquaporin-based diffusion. The high pH inside the chloroplast stroma (ca. 8) supports the carbonic anhydrase (CA)-catalysed conversion of CO_2 to HCO_3^- . Bicarbonate diffuses into the thylakoid through channels. The low pH inside the thylakoid (ca. 5) supports CA-catalysed conversion of HCO_3^- to CO_2 . The latter molecule diffuses into the pyrenoid where RubisCO is located.

Table 1

Model boundary conditions. Concentrations of CO_2 and HCO_3^- and pH in bulk seawater (temperature = 15 °C and salinity = 35), calculated from dissolved inorganic carbonate concentrations and pH measured by Rokitta and Rost (2012). The production rates of particulate organic and inorganic carbon (R_{POC} and R_{PIC}) measured by Rokitta and Rost (2012) constitute sinks for inorganic carbon. In terms of POC production, RubisCO fixes an additional amount of CO_2 that is released later-on into the cytosol via respiration (R_{R}). LLLC, LLHC, HLLC, and HLHC determine the four model experiments, where LL stands for low light ($50 \mu\text{mol photons} \cdot \text{m}^{-2} \cdot \text{s}^{-1}$), HL for high light ($300 \mu\text{mol photons} \cdot \text{m}^{-2} \cdot \text{s}^{-1}$), LC for low and HC for high carbon, respectively.

Model experiment	$[\text{CO}_2]^{\text{SW}} (\text{mol} \cdot \text{m}^{-3})$	$[\text{HCO}_3^-]^{\text{SW}} (\text{mol} \cdot \text{m}^{-3})$	pH	$R_{\text{POC}} + R_{\text{R}} (\text{mol} \cdot \text{cell}^{-1} \cdot \text{h}^{-1})$	$R_{\text{PIC}} (\text{mol} \cdot \text{cell}^{-1} \cdot \text{h}^{-1})$
LLLC	13×10^{-3}	1.9	8.1	$(35.4 + 5.59) \times 10^{-15}$	49.3×10^{-15}
LLHC	30×10^{-3}	2.2	7.8	$(65.6 + 1.64) \times 10^{-15}$	13×10^{-15}
HLLC	13×10^{-3}	1.9	8.1	$(82.8 + 24.8) \times 10^{-15}$	67.3×10^{-15}
HLHC	37×10^{-3}	2.1	7.7	$(92.1 + 6.45) \times 10^{-15}$	56.7×10^{-15}

gradient established during illumination drives H^+ out of the thylakoid, commonly through ATP synthetases. An import of H^+ into the thylakoid is effected by linear or cyclic electron transport (cf. Raven et al., 2014). Inside the thylakoid lumen (pH ca. 5), CA activity is assumed. In green algae, a CA was found that is associated to the thylakoid membrane (Pronina and Semenenko, 1983). RubisCO is located inside the pyrenoid (cf. Fig. 3) (Vaughn et al., 1990; Borkhsenius et al., 1998). The pyrenoid of *E. huxleyi* is closely surrounded by thylakoid stacks composed of three thylakoid layers (Billard and Inouye, 2004). For the model set-up, we assume that thylakoid and pyrenoid are closely associated to each other and form a so-termed thylakoid/pyrenoid complex. The CO_2 permeability between thylakoid/pyrenoid lumen and the chloroplast stroma is set to a low value (ten-times lower than the value measured by Prasad et al. (1998) for pure liposomemembranes) which may be achieved by the characteristic arrangement of thylakoid stacks and pyrenoid, but also by a specialised composition of the thylakoid membranes. The permeability coefficients of thylakoid membranes have not yet been determined to the best of our knowledge. RubisCO is located also inside the *in silico* thylakoid/pyrenoid complex.

Aiming to re-enact the experiment of Rokitta and Rost (2012) (matrix approach with two different light and CO_2 levels), the model is forced by four different external carbonate systems (Tab. 1), while setting the fixation rates of CO_2 into POC (inside the thylakoid/pyrenoid complex) and CO_3^{2-} into PIC (inside the CV) to the POC and PIC production values measured by Rokitta and Rost (2012). In terms of POC production, an additional amount of CO_2 is fixed that will be lost to respiration and thus be released into the cytosol. Respiration further provides the energy equivalents that are required for the $\text{Ca}^{2+}/\text{HCO}_3^-/\text{H}^+$ transport across the CV membrane and therewith regulates PIC production rates.

2.1. Mathematical implementation

2.1.1. Carbonate system

The carbonate system (CO_2 , HCO_3^- , CO_3^{2-} , H^+ , and OH^-) (cf. Zeebe and Wolf-Gladrow, 2001) is resolved dynamically for all four compartments.





The corresponding net reaction rates are denoted according to the numbers of the rate constants and describe the reactions (8) to (12) from right to left:

$$R_1 = -k_{+1}[\text{CO}_2] + k_{-1}[\text{H}^+][\text{HCO}_3^-] \quad (13)$$

$$R_4 = -k_{+4}[\text{OH}^-][\text{CO}_2] + k_{-4}[\text{HCO}_3^-] \quad (14)$$

$$R_5^{\text{H}^+} = -k_{+5}^{\text{H}^+}[\text{H}^+][\text{CO}_3^{2-}] + k_{-5}^{\text{H}^+}[\text{HCO}_3^-] \quad (15)$$

$$R_5^{\text{OH}^-} = -k_{+5}^{\text{OH}^-}[\text{OH}^-][\text{HCO}_3^-] + k_{-5}^{\text{OH}^-}[\text{CO}_3^{2-}][\text{H}_2\text{O}] \quad (16)$$

$$R_6 = -k_{+6} + k_{-6}[\text{H}^+][\text{OH}^-] \quad (17)$$

where concentrations are given in $\text{mol} \cdot \text{m}^{-3}$ and rates (R) in $\text{mol} \cdot \text{m}^{-3} \cdot \text{h}^{-1}$. For the chloroplast stroma and the thylakoid lumen, CA activity is assumed, i.e. R_1 (eqn.(13)) is multiplied by 10^4 (cf. Supuran and Scozzafava, 2007).

2.1.2. Differential equations

The cell model consists of 24 coupled differential equations that describe the rates by which the concentrations of CO_2 , HCO_3^- , CO_3^{2-} , H^+ , OH^- (in all compartments), Ca^{2+} and PIC (inside the CV), POC (inside the thylakoid lumen), and energy equivalents (EE, inside the cytosol) change. In the following, the differential equations are listed according to their compartmental affiliation, where concentrations are given in $\text{mol} \cdot \text{m}^{-3}$ and rates (R) in $\text{mol} \cdot \text{m}^{-3} \cdot \text{h}^{-1}$.

2.1.2.1. Cytosol (CS)

$$\begin{pmatrix} d[\text{CO}_2]^{\text{CS}}/dt \\ d[\text{HCO}_3^-]^{\text{CS}}/dt \\ d[\text{CO}_3^{2-}]^{\text{CS}}/dt \\ d[\text{H}^+]^{\text{CS}}/dt \\ d[\text{OH}^-]^{\text{CS}}/dt \\ d[\text{EE}]^{\text{CS}}/dt \end{pmatrix} = \begin{pmatrix} \text{C system} \\ 0 \end{pmatrix} + \begin{pmatrix} R_{\text{CO}_2,\text{PM}}^{\text{CS}} - R_{\text{CO}_2,\text{CVm}}^{\text{CS}} - R_{\text{CO}_2,\text{CPm}}^{\text{CS}} + R_{\text{R}} \\ R_{\text{HCO}_3^-,\text{PM}}^{\text{CS}} - R_{\text{Ca}^{2+},\text{CVm}}^{\text{CS}} \\ 0 \\ R_{\text{Ca}^{2+},\text{CVm}}^{\text{CS}} - R_{\text{H}^+,\text{PM}}^{\text{CS}} - R_{\text{H}^+,\text{CPm}}^{\text{CS}} \\ 0 \\ 4.5 R_{\text{R}} - \frac{1}{2} R_{\text{Ca}^{2+},\text{CVm}}^{\text{CS}} \end{pmatrix} \quad (18)$$

“C system” stands for carbonate system which is described by the reaction rates given in equations (13)–(17). $R_{\text{CO}_2,\text{PM}}$ stands for the CO_2 - $R_{\text{HCO}_3^-,\text{PM}}$ for the HCO_3^- , and $R_{\text{H}^+,\text{PM}}$ for the H^+ flux rate across the plasma membrane (1, 2, and 3 in Fig. 2). $R_{\text{CO}_2,\text{CVm}}$ gives the CO_2 flux rate and $R_{\text{Ca}^{2+},\text{CVm}}$ the flux rate of Ca^{2+} , HCO_3^- , and H^+ across the CV membrane (4 and 5 in Fig. 2). $R_{\text{CO}_2,\text{CPm}}$ and $R_{\text{H}^+,\text{CPm}}$ denote the CO_2 - and H^+ flux rate across the chloroplast envelope, respectively (6 and 7 in Fig. 2). R_{R} is the respiration rate that releases CO_2 into the cytosol while generating 4.5 energy equivalents (EE) per released CO_2 (13 in Fig. 2, value approximated for ATP production). R_{R} is chosen so that the generated energy equivalents which drive the import of Ca^{2+} and HCO_3^- for calcite precipitation into the CV suffice to reach the PIC production rates measured by Rokitta and Rost (2012).

2.1.2.2. Coccolith vesicle (CV)

$$\begin{pmatrix} d[\text{CO}_2]^{\text{CV}}/dt \\ d[\text{HCO}_3^-]^{\text{CV}}/dt \\ d[\text{CO}_3^{2-}]^{\text{CV}}/dt \\ d[\text{H}^+]^{\text{CV}}/dt \\ d[\text{OH}^-]^{\text{CV}}/dt \\ d[\text{Ca}^{2+}]^{\text{CV}}/dt \\ d[\text{PIC}]^{\text{CV}}/dt \end{pmatrix} = \begin{pmatrix} \text{C system} \\ 0 \\ 0 \end{pmatrix} + \begin{pmatrix} R_{\text{CO}_2,\text{CVm}}^{\text{CV}} \\ R_{\text{Ca}^{2+},\text{CVm}}^{\text{CV}} \\ -R_{\text{P}} \\ -R_{\text{Ca}^{2+},\text{CVm}}^{\text{CV}} \\ 0 \\ R_{\text{Ca}^{2+},\text{CVm}}^{\text{CV}} - R_{\text{P}} \\ R_{\text{P}} \end{pmatrix} \quad (19)$$

where R_{P} stands for the precipitation rate (11 in Fig. 2).

2.1.2.3. Chloroplast stroma (CPstr)

$$\begin{pmatrix} d[\text{CO}_2]^{\text{CPstr}}/dt \\ d[\text{HCO}_3^-]^{\text{CPstr}}/dt \\ d[\text{CO}_3^{2-}]^{\text{CPstr}}/dt \\ d[\text{H}^+]^{\text{CPstr}}/dt \\ d[\text{OH}^-]^{\text{CPstr}}/dt \end{pmatrix} = \begin{pmatrix} \text{C system} \end{pmatrix} + \begin{pmatrix} R_{\text{CO}_2,\text{CPm}}^{\text{CPstr}} - R_{\text{CO}_2,\text{thyl}}^{\text{CPstr}} \\ -R_{\text{HCO}_3^-,\text{thyl}}^{\text{CPstr}} \\ 0 \\ R_{\text{H}^+,\text{CPm}}^{\text{CPstr}} - R_{\text{H}^+,\text{thyl}}^{\text{CPstr}} \\ 0 \end{pmatrix} \quad (20)$$

where the “C system” includes CA activity (cf Section 2.1.1). $R_{\text{CO}_2,\text{thyl}}$, $R_{\text{HCO}_3^-,\text{thyl}}$ and $R_{\text{H}^+,\text{thyl}}$ indicate the fluxes of CO_2 , HCO_3^- and H^+ between chloroplast stroma and thylakoid lumen (8, 9, and 10 in Fig. 2).

2.1.2.4. Thylakoid lumen (thyl)

$$\begin{pmatrix} d[\text{CO}_2]^{\text{thyl}}/dt \\ d[\text{HCO}_3^-]^{\text{thyl}}/dt \\ d[\text{CO}_3^{2-}]^{\text{thyl}}/dt \\ d[\text{H}^+]^{\text{thyl}}/dt \\ d[\text{OH}^-]^{\text{thyl}}/dt \\ d[\text{POC}]^{\text{thyl}}/dt \end{pmatrix} = \begin{pmatrix} \text{C system} \\ 0 \end{pmatrix} + \begin{pmatrix} R_{\text{CO}_2}^{\text{thyl}} - R_{\text{CO}_2}^{\text{RubisCO}} \\ 0 \\ 0 \\ R_{\text{H}^+}^{\text{thyl}} \\ 0 \\ R_{\text{CO}_2}^{\text{RubisCO}} \end{pmatrix} \quad (21)$$

where the “C system” also includes CA activity $R_{\text{CO}_2}^{\text{RubisCO}}$ gives the CO_2 fixation rate by RubisCO (12 in Fig. 2) which is set to the POC production rate measured by Rokitta and Rost (2012) plus the respiration rate R_{R} .

2.1.3. Flux rates

For the calculation of some fluxes, we use smooth cut-off functions (fun_X) that rely on the following structure:

$$\text{fun}_X = Y_i \cdot \tanh(X - X_i) + Y_{ii} \quad (22)$$

where X denotes the variable value such as for instance the cytosolic pH in equation (25), X_i indicates the X value, where the strongest change in fun_X occurs. Y_i and Y_{ii} define the size range of fun_X . Values for X_i , Y_i , and Y_{ii} are given in Table 2.

In the following, flux rate calculations are listed in the order of the numbers allocated in Figure 2. Concentrations are given in $\text{mol} \cdot \text{m}^{-3}$, rates in $\text{mol} \cdot \text{m}^{-3} \cdot \text{h}^{-1}$, permeability coefficients (γ) in $\text{m} \cdot \text{h}^{-1}$, volumes (V) in m^3 , and surface areas (A) in m^2 . External concentrations of CO_2 , HCO_3^- and H^+ are listed in Table 1. Volumes and surface areas of the four compartments are listed in Table 3. Physiological parameter values and a description of the parameters are given in Table 4.

(1) CO_2 flux across plasma membrane

$R_{\text{CO}_2,\text{PM}}^{\text{CS}}$ gives the rate by which the CO_2 concentration inside the cytosol (CS) changes due to CO_2 diffusion across the plasma membrane (PM).

$$R_{\text{CO}_2,\text{PM}}^{\text{CS}} = \gamma_{\text{CO}_2,\text{PM}}^{\text{CS}} \cdot \frac{A^{\text{CS}}}{V^{\text{CS}}} \cdot ([\text{CO}_2]^{\text{SW}} - [\text{CO}_2]^{\text{CS}}) \quad (23)$$

(2) HCO_3^- flux across plasma membrane

$$R_{\text{HCO}_3^-,\text{PM}}^{\text{CS}} = \gamma_{\text{HCO}_3^-,\text{PM}}^{\text{CS}} \cdot \frac{A^{\text{CS}}}{V^{\text{CS}}} \cdot ([\text{HCO}_3^-]^{\text{SW}} - [\text{HCO}_3^-]^{\text{CS}}) \quad (24)$$

(3) Proton flux across plasma membrane

Protons enter or leave the cell in order to keep cytosolic pH close to 7. The rate by which the H^+ concentration inside the cytosol changes is:

$$R_{\text{H}^+,\text{PM}}^{\text{CS}} = \text{fun}_{\text{H}^+} \cdot R_{\text{max},\text{PM}}^{\text{H}^+} \quad (25)$$

(4.) CO₂ flux across coccolith vesicle membrane

$$R_{\text{CO}_2, \text{CVm}}^{\text{CV}} = \gamma_{\text{CO}_2, \text{CVm}} \cdot \frac{A^{\text{CV}}}{\sqrt{V^{\text{CV}}}} \cdot ([\text{CO}_2]^{\text{CS}} - [\text{CO}_2]^{\text{CV}}) \quad (26)$$

The corresponding rate for the cytosol reads:

$$R_{\text{CO}_2, \text{CVm}}^{\text{CS}} = R_{\text{CO}_2, \text{CVm}}^{\text{CV}} \cdot \frac{V^{\text{CV}}}{\sqrt{V^{\text{CS}}}} \quad (27)$$

Table 2

Parameter values for the cut-off functions. The basic structure of the functions is given by eqn. (22). The concentrations of Ca²⁺, energy equivalents (EE), and HCO₃⁻ are given in mol · m⁻³. CPstr - chloroplast stroma, CS - cytosol, CV - coccolith vesicle, thyl - thylakoid lumen, column "eqn." hints at the equations, in which the cut-off functions are used.

Function	X	X _i	Y _i	Y _{ii}	eqn.
fun _{Ca²⁺}	-100 · [Ca ²⁺] ^{CV}	-10 ³	0.5	0.5	(28)
fun _{EE}	100 · [EE] ^{CS}	2 × 10 ⁴	0.5	0.5	(28)
fun _{H⁺}	pH ^{CS}	7	-1	0	(25)
fun _{H₂⁺}	pH ^{CPstr}	8	-1	0	(32)
fun _{H₃⁺}	pH ^{thyl}	5	-1	0	(38)
fun _{HCO₃⁻}	10 · [HCO ₃ ⁻] ^{CS}	0.3	0.5	0.5	(28)

Table 3

Morphological parameter values used for the cell model. CP - chloroplast, CPstr - chloroplast stroma, CS - cytosol, CV - coccolith vesicle, PM - plasma membrane, thyl - thylakoid lumen, thyl - thylakoid/pyrenoid complex.

Parameter (unit)	Description	value
V ^{CS} (m ³)	Volume CS	16.1 × 10 ⁻¹⁸
A ^{CS} (m ²)	PM amount	78.5 × 10 ⁻¹²
V ^{CV} (m ³)	Volume CV	1.6 × 10 ⁻¹⁸
A ^{CV} (m ²)	Membrane surrounding CV	16.8 × 10 ⁻¹²
V ^{CP} (m ³)	Volume of (bulk) CP	28.3 × 10 ⁻¹⁸
V ^{CPstr} (m ³)	Volume of CPstr	22.6 × 10 ⁻¹⁸
A ^{CP} (m ²)	Membrane surrounding CP	64.1 × 10 ⁻¹²
V ^{thyl} (m ³)	Volume of thylakoid	5.7 × 10 ⁻¹⁸
A ^{thyl} (m ²)	Membrane surrounding thylakoid	37 × 10 ⁻¹²

Table 4

Physiological parameter values for the model. AQP - aquaporin, CPm - chloroplast envelope, CPstr - chloroplast stroma, CV - coccolith vesicle, CVm - CV membrane, POC - particulate organic carbon, PON - particulate organic nitrogen, PM - plasma membrane. LLLC, LLHC, HLLC, and HLHC denote the four model experiments where LL stands for low light, HL for high light, LC for low and HC for high carbon.

Parameter (unit)	Description	LLLC	LLHC	HLLC	HLHC
γ _{CO₂,CPm} (m · h ⁻¹)	Permeability coefficient of CPm for CO ₂	0.1	Uehlein et al. (2008)		
γ _{CO₂,CVm} (m · h ⁻¹)	Permeability coefficient of CVm for CO ₂ (no AQPs)	0.02	Prasad et al. (1998)		
γ _{CO₂,PM} (m · h ⁻¹)	AQP-based permeability coefficient of PM for CO ₂	0.31	Uehlein et al. (2008)		
γ _{CO₂,thyl} (m · h ⁻¹)	Permeability coefficient of thylakoid/pyrenoid complex for CO ₂	0.002			
γ _{HCO₃⁻,PM} (m · h ⁻¹)	Permeability coefficient of PM for HCO ₃ ⁻	0.0016			
γ _{HCO₃⁻,thyl} (m · h ⁻¹)	Permeability coefficient of thylakoid/pyrenoid complex for CO ₂	0.02			
K _{m, Ca²⁺/HCO₃⁻/H⁺} (mol · m ⁻³)	Half saturation constant of Ca ²⁺ /HCO ₃ ⁻ /H ⁺ transporter towards cytosolic [Ca ²⁺]	10 ⁻³			
k _f (mol · m ⁻³ · h ⁻¹)	Calcite precipitation related rate constant	110 × 10 ⁻⁹	Zuddas and Mucci (1994)		
n	Calcite precipitation related parameter	2.35	Zuddas and Mucci (1994)		
R _{max,CPm} ^{H⁺} (mol · m ⁻³ · h ⁻¹)	Maximum rate by which [H ⁺] in CPstr changes due to H ⁺ fluxes across CPm	1.94 × 10 ⁸			
R _{max,PM} ^{H⁺} (mol · m ⁻³ · h ⁻¹)	Maximum rate by which [H ⁺] in CS changes due to H ⁺ fluxes across PM	1.7 × 10 ⁶			
R _{max,thyl} ^{H⁺} (mol · m ⁻³ · h ⁻¹)	Maximum rate by which [H ⁺] in thylakoid lumen changes	3.95 × 10 ⁸			
R _{POC} (mol · cell ⁻¹ · h ⁻¹)	Net POC production rate Rokitta and Rost (2012)	35.4 × 10 ⁻¹⁵	65.5 × 10 ⁻¹⁵	82.8 × 10 ⁻¹⁵	92.1 × 10 ⁻¹⁵
R _R (mol · cell ⁻¹ · h ⁻¹)	Respiration rate	5.59 × 10 ⁻¹⁵	1.64 × 10 ⁻¹⁵	24.8 × 10 ⁻¹⁵	6.45 × 10 ⁻¹⁵
V _{max, Ca²⁺/HCO₃⁻/H⁺} (mol · h ⁻¹)	Maximal transport velocity of Ca ²⁺ /HCO ₃ ⁻ /H ⁺ transporter	0.72 × 10 ⁻¹²			

R_{CO₂,CVm}^{CS} is subtracted from the cytosolic CO₂ pool, when R_{CO₂,CVm}^{CV} is added to the CV-internal CO₂ pool (cf. eqns. (18) and (19)).

- (5.) Ca²⁺/HCO₃⁻/H⁺ fluxes across coccolith vesicle membrane
Calcium ions can be accumulated within the CV up to a CV-internal concentration of 10 mol · m⁻³ (fun_{Ca²⁺}) as previously presumed in [Holtz et al. \(2013\)](#). Furthermore, the Ca²⁺/HCO₃⁻/H⁺ transport (stoichiometry: 1:1:1, cf. (eqns. (18) and 19)) is made dependent on the availability of cytosolic HCO₃⁻ and energy equivalents (fun_{HCO₃⁻}, fun_{EE}). The rate by which the Ca²⁺ concentration inside the CV changes is:

$$R_{\text{Ca}^{2+}, \text{CVm}}^{\text{CV}} = \text{fun}_{\text{Ca}^{2+}} \cdot \text{fun}_{\text{HCO}_3^-} \cdot \text{fun}_{\text{EE}} \cdot \frac{1}{\sqrt{V^{\text{CV}}}} \cdot \frac{V_{\text{max, Ca}^{2+}/\text{HCO}_3^-/\text{H}^+} \cdot [\text{Ca}^{2+}]^{\text{CS}}}{K_{\text{m, Ca}^{2+}/\text{HCO}_3^-/\text{H}^+} + [\text{Ca}^{2+}]^{\text{CS}}} \quad (28)$$

For the cytosol, the rate is:

$$R_{\text{Ca}^{2+}, \text{CVm}}^{\text{CS}} = R_{\text{Ca}^{2+}, \text{CVm}}^{\text{CV}} \cdot \frac{V^{\text{CV}}}{\sqrt{V^{\text{CS}}}} \quad (29)$$

The Ca²⁺ concentration inside the cytosol ([Ca²⁺]^{CS}) is set to a fixed value, i.e. 10⁻⁴ mol · m⁻³ ([Brownlee et al., 1995](#)).

- (6.) CO₂ flux across chloroplast envelope

$$R_{\text{CO}_2, \text{CPm}}^{\text{CPstr}} = \gamma_{\text{CO}_2, \text{CPm}} \cdot \frac{A^{\text{CP}}}{\sqrt{V^{\text{CPstr}}}} \cdot ([\text{CO}_2]^{\text{CS}} - [\text{CO}_2]^{\text{CPstr}}) \quad (30)$$

The corresponding rate for the cytosol reads:

$$R_{\text{CO}_2, \text{CPm}}^{\text{CS}} = R_{\text{CO}_2, \text{CPm}}^{\text{CPstr}} \cdot \frac{V^{\text{CPstr}}}{\sqrt{V^{\text{CS}}}} \quad (31)$$

- (7.) Proton flux across chloroplast envelope

Protons enter or leave the chloroplast stroma in order to keep the pH close to 8 (fun_{H⁺}²).

$$R_{\text{H}^+, \text{CPm}}^{\text{CPstr}} = \text{fun}_{\text{H}_2^+} \cdot R_{\text{max,CPm}}^{\text{H}^+} \quad (32)$$

The corresponding rate for the cytosol reads:

$$R_{\text{H}^+, \text{CPm}}^{\text{CS}} = R_{\text{H}^+, \text{CPm}}^{\text{CPstr}} \cdot \frac{V^{\text{CPstr}}}{\sqrt{V^{\text{CS}}}} \quad (33)$$

(8.) HCO_3^- flux between chloroplast stroma and thylakoid lumen

$$R_{\text{HCO}_3^-}^{\text{thyl}} = \gamma_{\text{HCO}_3^-, \text{thyl}} \cdot \frac{A^{\text{thyl}}}{V^{\text{thyl}}} \cdot ([\text{HCO}_3^-]^{\text{CPstr}} - [\text{HCO}_3^-]^{\text{thyl}}) \quad (34)$$

The corresponding rate for the chloroplast stroma reads:

$$R_{\text{HCO}_3^-}^{\text{CPstr}} = R_{\text{HCO}_3^-}^{\text{thyl}} \cdot \frac{V^{\text{thyl}}}{V^{\text{CPstr}}} \quad (35)$$

(9.) CO_2 flux between chloroplast stroma and thylakoid lumen

$$R_{\text{CO}_2}^{\text{thyl}} = \gamma_{\text{CO}_2, \text{thyl}} \cdot \frac{A^{\text{thyl}}}{V^{\text{thyl}}} \cdot ([\text{CO}_2]^{\text{CPstr}} - [\text{CO}_2]^{\text{thyl}}) \quad (36)$$

The corresponding rate for the chloroplast stroma reads:

$$R_{\text{CO}_2}^{\text{CPstr}} = R_{\text{CO}_2}^{\text{thyl}} \cdot \frac{V^{\text{thyl}}}{V^{\text{CPstr}}} \quad (37)$$

(10.) Proton flux between chloroplast stroma and thylakoid lumen
Protons enter or leave the thylakoid lumen in order to keep the pH of the thylakoid lumen close to 5 (fun_{H^+}).

$$R_{\text{H}^+, \text{thyl}}^{\text{thyl}} = \text{fun}_{\text{H}^+} \cdot R_{\text{max}, \text{thyl}}^{\text{H}^+} \quad (38)$$

The corresponding rate for the chloroplast stroma reads:

$$R_{\text{H}^+, \text{thyl}}^{\text{CPstr}} = R_{\text{H}^+, \text{thyl}}^{\text{thyl}} \cdot \frac{V^{\text{thyl}}}{V^{\text{CPstr}}} \quad (39)$$

(11.) Calcite precipitation inside coccolith vesicle
Calcite is precipitated from Ca^{2+} and CO_3^{2-} :

The corresponding precipitation rate (after Zuddas and Mucci, 1994) is:

$$R_{\text{P}} = \begin{cases} k_f(\Omega - 1)^n & \text{for } \Omega > 1 \\ 0 & \text{for } \Omega \leq 1 \end{cases} \quad (41)$$

where Ω is the calcite saturation product that is dependent on the prevailing concentrations of Ca^{2+} and CO_3^{2-} . The parameter n is given in Zuddas and Mucci (1994), and k_f can be calculated (cf. Zuddas and Mucci, 1994; Holtz et al., 2013).

(12.) CO_2 fixation inside thylakoid/pyrenoid complex
The CO_2 fixation rate of RubisCO ($R_{\text{CO}_2}^{\text{RubisCO}}$) is calculated as follows:

$$R_{\text{CO}_2}^{\text{RubisCO}} = \frac{1}{V^{\text{thyl}}} (R_{\text{POC}} + R_{\text{R}}) \quad (42)$$

(13.) Respiration inside cytosol

Respiration releases CO_2 into the cytosol with the following rate.

$$R_{\text{R}} = \frac{1}{V^{\text{CS}}} R_{\text{R}} \quad (43)$$

3. Results

The model was run into steady state, i.e. until all state variables remained constant over time. The values calculated for experiments LLLC, LLHC, and HLHC are listed in Table 5. The CO_2 and HCO_3^- concentration gradients that are obtained direct from seawater across the cytoplasm into the chloroplast stroma. While CO_2 can diffuse across the plasma membrane and the chloroplast envelope, HCO_3^- cannot cross the chloroplast envelope in our

Table 5

Calculated steady state values inside the four model compartments. Concentrations are given in $\text{mol} \cdot \text{m}^{-3}$, Ω is dimensionless. LLLC, LLHC, and HLHC denote the three model experiments that can be explained by the fluxes proposed in Fig. 2 where LL stands for low light, HL for high light, LC for low and HC for high carbon.

	LLC	LLHC	HLHC
Cytoplasm			
pH	7.00	7.00	7.00
CO_2	11.7×10^{-3}	27.8×10^{-3}	33.4×10^{-3}
HCO_3^-	1.44	2.03	1.61
CO_3^{2-}	10.2×10^{-3}	14.4×10^{-3}	11.4×10^{-3}
Coccolith vesicle			
pH	8.62	8.32	8.34
CO_2	11.7×10^{-3}	27.8×10^{-3}	33.4×10^{-3}
HCO_3^-	5.12	6.22	7.74
CO_3^{2-}	1.46	0.915	1.16
Ca^{2+}	3.10	3.10	4.11
Ω	12.1	7.59	12.8
Chloroplast stroma			
pH	8.00	8.00	8.00
CO_2	5.5×10^{-3}	17.6×10^{-3}	18.5×10^{-3}
HCO_3^-	77.3×10^{-3}	0.323	0.307
CO_3^{2-}	5.49×10^{-3}	23.0×10^{-3}	21.8×10^{-3}
Thylakoid/pyrenoid complex			
pH	5.00	5.00	5.00
CO_2	0.101	1.10	0.818
HCO_3^-	12.7×10^{-3}	0.124	94.4×10^{-3}
CO_3^{2-}	0.9×10^{-6}	8.9×10^{-6}	6.8×10^{-6}

model. Inside the thylakoid/pyrenoid complex, the HCO_3^- concentration is lower than inside the chloroplast stroma, while CO_2 is strongly accumulated. The passage of HCO_3^- across the thylakoid/pyrenoid complex-confining membrane is facilitated via channels; CO_2 diffusion, in contrast, is low.

Under high light intensities and low external CO_2 concentrations (HLLC), some of the state variable concentrations inside the chloroplast become negative when using the parameter set given in Table 4 and the model does not reach steady state until the end of the model run (three days in total). It follows that cellular carbon fluxes under HLLC conditions cannot be explained by the fluxes proposed in Figure 2. A hypothesis will be developed in the discussion section (Section 4.2) that considers the variation of cellular carbon fluxes under different light and CO_2 conditions and hence includes fluxes under HLLC conditions.

4. Discussion

The discussion is presented in the sequence of the three questions posed at the end of the introduction.

4.1. Can CO_2 and HCO_3^- pass the cytosol without being inter-converted?

The bulk of experiments conducted until today gives evidence that POC production in *E. huxleyi* is basically fed by external CO_2 and external HCO_3^- and that PIC production is fed by external HCO_3^- only. Thus, we suggested in the beginning that CO_2 is rarely converted to HCO_3^- within the cytosol, because PIC production seems to be fed by external HCO_3^- only.

Compared to influx rates of CO_2 and HCO_3^- , calculated inter-conversion rates between cytosolic CO_2 and HCO_3^- are low (Tab. 6). Due to the higher concentrations of HCO_3^- compared to CO_2 , conversion rates of HCO_3^- to CO_2 are higher than those of the inverse reaction. As mentioned above, the carbon demand of photosynthesis in experiment HLLC cannot be covered by means of the carbon fluxes proposed in Figure 2. We find that neither

Table 6

Inter-conversion rates between cytosolic CO_2 and HCO_3^- as percentage of the influx of CO_2 and HCO_3^- , respectively. Rel. conv. of CO_2 to HCO_3^- (%) - conversion rate of cytosolic CO_2 into HCO_3^- as percentage of cellular CO_2 influx; Rel. conv. of HCO_3^- to CO_2 (%) - conversion rate of cytosolic HCO_3^- into CO_2 as percentage of HCO_3^- cellular influx. LLLC, LLHC, and HLHC denote the three model experiments that lead to reasonable results where LL stands for low light, HL for high light, LC for low and HC for high carbon.

	LLLC	LLHC	HLHC
Rel. conv. of CO_2 to HCO_3^- (%)	0.03	0.04	0.03
Rel. conv. of HCO_3^- to CO_2 (%)	0.24	1.16	0.24

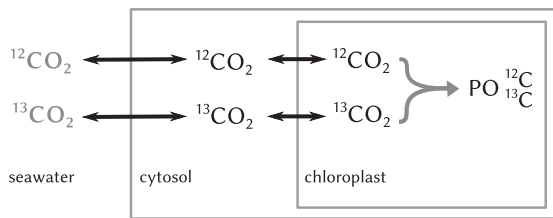


Fig. 4. Stable carbon isotope model. $^{12}\text{CO}_2$ and $^{13}\text{CO}_2$ diffuse independently of each other across plasma membrane and chloroplast envelope. The chloroplast is surrounded by three membranes which is not indicated in the figure. Inside the chloroplast, CO_2 is fixed into particulate organic carbon (POC) with the rates measured by Rost et al. (2002). The concentrations of external $^{12}\text{CO}_2$ and $^{13}\text{CO}_2$ were measured by Rost et al. (2002) also.

CA-activity nor strong HCO_3^- accumulation ($> 150 \text{ mol} \cdot \text{m}^{-3}$) inside the cytosol are able to provide photosynthesis with enough CO_2 stemming from cytosolic HCO_3^- conversion. Assuming both at a time, CA-activity and HCO_3^- accumulation inside the cytosol ($\sim 150 \text{ mol} \cdot \text{m}^{-3}$), carbon provision from cytosolic HCO_3^- conversion suffices to cover the demand of photosynthesis in experiment HLLC. Under these conditions, however, around 99% of the imported HCO_3^- is lost from the cell via CO_2 diffusion which would imply very high energy demands. An alternative, more energy-efficient carbon pathway will be proposed in Section 4.2 (cf. Fig. 5).

4.2. Can enough external CO_2 be taken up by diffusion to satisfy the carbon requirement of POC production?

Diffusive CO_2 influx relies on a CO_2 concentration gradient from the external medium into the cytoplasm. In our model, such a gradient is established via an energy-efficient, chloroplast-based CCM that relies on internal pH gradients, CA-activity inside the chloroplast stroma and the thylakoid lumen, CO_2 fixation by RubisCO, HCO_3^- channels inside the thylakoid membrane, and differences in CO_2 permeabilities between the various membranes (for a review on energy-costs of CCMs see Raven et al., 2014).

Carbon dioxide permeabilities of plasma membrane and chloroplast envelope play a decisive role for the diffusive influx of CO_2 . Our calculations are based on the CO_2 permeability coefficient determined for the plasma membrane of *N. tabacum* that is known to include aquaporins ($0.31 \text{ m} \cdot \text{h}^{-1}$) (Uehlein et al., 2008). On basis of the (lower) CO_2 permeability coefficients determined for *Chlamydomonas reinhardtii* ($0.03 - 0.06 \text{ m} \cdot \text{h}^{-1}$) (Sültemeyer and Rinast, 1996) and for artificial membranes that contain aquaporins from human erythrocytes ($0.07 \text{ m} \cdot \text{h}^{-1}$) (Prasad et al., 1998), calculated fluxes of external CO_2 towards RubisCO are lower than the POC production rates determined by Rokitta and Rost (2012) in all four model simulations. It follows that the proposed CCM depends on comparably high CO_2 permeabilities of the plasma membrane and the chloroplast envelope. These permeabilities have not yet been determined for *E. huxleyi*. The CO_2 permeability coefficients determined by Hopkinson et al. (2011) for the plasma membranes of different diatom species, however, are in the range

from 0.54 to $2 \text{ m} \cdot \text{h}^{-1}$ and thus exceed the value used in our model. Nevertheless, using even the highest permeability value determined by Hopkinson et al. (2011) does not lead to sufficiently high carbon fluxes in model experiment HLLC.

In contrast to our assumption that CO_2 enters the cell following its concentration gradient, some authors (e.g. Schulz et al., 2007) assume that CO_2 leaves the cell of *E. huxleyi* following a concentration gradient that is established via an active import of CO_2 . This CO_2 efflux is thought to support the export of $^{13}\text{CO}_2$ that accumulates inside the cell due to RubisCO's fractionation against $^{13}\text{CO}_2$. A simple two-compartment model is established (Fig. 4) to test whether a net efflux of $^{13}\text{CO}_2$ is necessary for the cell to dispose of ^{13}C that accumulates around RubisCO.

The model takes into account diffusive fluxes of $^{12}\text{CO}_2$ and $^{13}\text{CO}_2$ between medium/seawater, cytosol, and "bulk chloroplast" (i.e. chloroplast is not divided into chloroplast stroma and thylakoid/pyrenoid complex as in the other model). Inside the bulk chloroplast, $^{12}\text{CO}_2$ and $^{13}\text{CO}_2$ are fixed into POC with the rates measured by Rost et al. (2002). Rost et al. (2002) measured the fixation rates of ^{12}C and ^{13}C into POC in dependence on different external $^{12}\text{CO}_2$ and $^{13}\text{CO}_2$ concentrations and light conditions. The mathematical implementation of our model is given in the Appendix.

The model shows that *E. huxleyi* does not rely on a net efflux of $^{13}\text{CO}_2$ in order to dispose of the $^{13}\text{CO}_2$ that may accumulate inside the cell due to RubisCO's fractionation against $^{13}\text{CO}_2$. Calculated concentration gradients for $^{12}\text{CO}_2$ and $^{13}\text{CO}_2$ direct from the external medium/seawater into the bulk chloroplast (Tab. 7) and the resulting CO_2 influx has a lower $^{13}\text{R}_{\text{CO}_2}$ ($[^{13}\text{CO}_2]:[^{12}\text{CO}_2]$) than the external medium ($\Delta^{13}\text{R}_{\text{CO}_2,\text{infl}}$ in Tab. 7), because the ratio between the $^{13}\text{CO}_2$ fixation rate of RubisCO and the external $^{13}\text{CO}_2$ concentration is lower than the same ratio for $^{12}\text{CO}_2$.

For 29 out of 35 model experiments, the model shows that diffusive CO_2 uptake can explain the POC production rates measured by Rost et al. (2002) (Tab. 7). The remaining six data points (italic numbers in Tab. 7) represent experiments that were conducted under low external CO_2 concentrations and high light intensities which is well in line with the findings presented in Section 4.2 for the cell model. We hence argue that whether diffusive CO_2 uptake can cover the carbon demand of RubisCO or not depends on the light intensity on the one hand and on the availability of external CO_2 on the other. In case the carbon demand of RubisCO cannot be covered by CO_2 diffusion only, we propose an additional uptake of HCO_3^- (cf. hypothesis presented in Fig. 5) which is in line with the findings of Rost et al. (2002); Bach et al. (2013), and Kottmeier et al.: The stable carbon isotope composition of POC measured by Rost et al. (2002) under different light and CO_2 levels can be explained by an additional uptake of HCO_3^- when CO_2 availability is low. Bach et al. (2013) showed by means of transcriptome analyses that anion exchangers that are presumably involved in HCO_3^- uptake are upregulated under low external DIC concentrations. Kottmeier et al. measured HCO_3^- usage for POC production only under low external CO_2 concentrations. Under high CO_2 concentrations, POC production relies on CO_2 uptake exclusively. As shown in Section 4.1, high conversion rates of cytosolic HCO_3^- to CO_2 that could feed the chloroplast with CO_2 are dependent on CA-activity and a very high HCO_3^- accumulation inside the cytosol which would then lead to very high CO_2 efflux rates. An additional uptake of HCO_3^- into the cytosol and from there into the chloroplast would certainly constitute the more energy-efficient possibility to import carbon. According to the state variable concentrations in steady state calculated for the four model compartments (Tab. 5), HCO_3^- could even follow its concentration gradient into the chloroplast.

To sum up, depending on the CO_2 permeabilities of plasma membrane and chloroplast envelope, CO_2 for POC production can be taken up via diffusion under LLLC, LLHC, and HLHC, but not under HLLC conditions.

Table 7

Model outputs to stable carbon isotope model. $^{12}\text{CO}_2$ and $^{13}\text{CO}_2$ concentrations in the cytosol (CS, in steady state), and the bulk chloroplast (CP). All concentrations are given in $\text{mmol} \cdot \text{m}^{-3}$. Negative concentrations inside the chloroplast indicate that a diffusive influx of external CO_2 cannot be the only carbon source for POC production. L:D - light:dark cycle (unit: h:h); PFD - photon flux density (unit: $\mu\text{mol photons} \cdot \text{m}^{-2} \cdot \text{s}^{-1}$). $\Delta^{13}\text{R}_{\text{CO}_2,\text{infl}}$ stands for: $10^3 \cdot ([^{13}\text{CO}_2] : [^{12}\text{CO}_2])_{\text{ext. medium}} - ([^{13}\text{CO}_2] : [^{12}\text{CO}_2])_{\text{cell. infl}}$; a positive value thus indicates that $[^{13}\text{CO}_2] : [^{12}\text{CO}_2]$ of ext. medium exceeds $[^{13}\text{CO}_2] : [^{12}\text{CO}_2]$ of cellular CO_2 influx. Numbers set in *italic* indicate the six experiments that cannot be explained by the model.

L:D	PFD	CS		CP		$\Delta^{13}\text{R}_{\text{CO}_2,\text{infl}}$
		$^{12}\text{CO}_2$	$^{13}\text{CO}_2$	$^{12}\text{CO}_2$	$^{13}\text{CO}_2$	
24:0	15	32.6	0.363	29.7	0.331	0.166
		29.3	0.326	26.7	0.297	0.163
		18.3	0.203	15.6	0.174	0.161
		18.9	0.211	16.2	0.181	0.160
		12.3	0.137	9.7	0.109	0.174
	30	25.4	0.282	19.4	0.217	0.168
		21.6	0.241	16.4	0.184	0.175
		17.1	0.191	12.4	0.139	0.170
		15.3	0.171	10.3	0.115	0.173
		10.6	0.118	6.5	0.073	0.178
	80	25.4	0.284	12.8	0.146	0.185
		24.2	0.270	13.9	0.157	0.187
		16.6	0.186	6.9	0.079	0.195
		16.8	0.187	8.2	0.093	0.184
		9.4	0.105	1.6	0.019	0.178
	150	27.0	0.300	17.0	0.192	0.193
		19.9	0.222	11.1	0.126	0.187
		14.8	0.165	4.3	0.050	0.187
		14.0	0.157	4.6	0.053	0.191
		9.3	0.104	1.0	0.013	0.185
16:8	30	30.6	0.340	26.2	0.292	0.086
		22.4	0.249	18.2	0.203	0.074
		14.0	0.155	6.4	0.072	0.083
		9.2	0.103	3.5	0.040	0.074
		4.0	0.045	-0.6	-0.006	0.085
	80	28.0	0.312	13.8	0.156	0.107
		19.6	0.219	3.8	0.045	0.113
		12.6	0.141	-0.1	-26×10^{-6}	0.087
		9.0	0.101	-3.2	-0.034	0.107
		3.0	0.033	-6.2	-0.067	0.096
	150	23.9	0.266	12.9	0.145	0.131
		17.8	0.198	5.8	0.067	0.131
		15.3	0.171	4.7	0.054	0.131
		9.3	0.104	-1.7	-0.017	0.119
		2.8	0.031	-7.3	-0.080	0.101

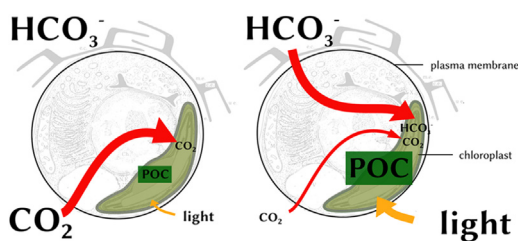


Fig. 5. Hypothesis concerning the usage of CO_2 and HCO_3^- for POC production. Under high external $[\text{CO}_2]$ and low light intensities (left), POC is built from external CO_2 which diffuses into the cell. Under low external $[\text{CO}_2]$ and high light intensities (right), provision of POC production with CO_2 via diffusion is insufficient. Thus, HCO_3^- is taken up as well to provide POC production with CO_2 . Illustration includes drawing of van der Wal et al. (1983).

4.3. Can CO_2 be accumulated around RubisCO without inorganic carbon species being transported against concentration gradients?

In the cell model, CO_2 diffuses across plasma membrane and chloroplast envelope into the chloroplast stroma. Inside the alkaline chloroplast stroma, CA-catalysed CO_2 conversion leads to HCO_3^- accumulation. Bicarbonate ions enter the acidic thylakoid lumen through channels and are converted by CA activity to CO_2 . Inside the thylakoid lumen, CO_2 is fixed into POC with the rates

measured by Rokitta and Rost (2012) (plus the additional amount that will be lost again to respiration inside the cytosol).

Calculated CO_2 concentrations inside the thylakoid (Tab. 5) not only exceed external CO_2 concentrations (Tab. 1) but also the half saturation constant K_m of RubisCO ($0.072 \text{ mol} \cdot \text{m}^{-3}$, Boller et al., 2011). Thus, under LLC, LLHC, and HLHC conditions, the implemented CCM leads to strong CO_2 accumulation around RubisCO without inorganic carbon species being transported against a concentration gradient.

5. Conclusion

A numerical cell model was implemented that proposes an energy-efficient possibility to take up inorganic carbon for POC and PIC production. We find (1) that CO_2 and HCO_3^- do rarely inter-convert during their passage of the cytosol, (2) that CO_2 for photosynthesis can be taken up via diffusion under high CO_2 concentrations and nonsaturating light conditions, (3) that a CCM can lead to CO_2 accumulation around RubisCO without a transport of inorganic carbon species against concentration gradients, and (4) that CO_2 does not have to leave the cell in order to dispose of $^{13}\text{CO}_2$ that accumulates intracellularly due to RubisCO's fractionation. Under low external CO_2 concentrations and high light intensities, the carbon demand of photosynthesis cannot be

Table 8

Model inputs. $^{12}\text{CO}_2$ and $^{13}\text{CO}_2$ concentrations (unit here: $\text{mmol} \cdot \text{m}^{-3}$, unit for implementation: $\text{mol} \cdot \text{m}^{-3}$) in the medium (SW, set constant in the model, measured by Rost et al. (2002)) and the fixation rates of $^{12}\text{CO}_2$ and $^{13}\text{CO}_2$ into PO^{12}C and PO^{13}C , respectively ($R_{\text{PO}^{12}\text{C}}$ and $R_{\text{PO}^{13}\text{C}}$, unit here: $\text{fmol} \cdot \text{cell}^{-1} \cdot \text{h}^{-1}$, unit for implementation: $\text{mol} \cdot \text{cell}^{-1} \cdot \text{h}^{-1}$). CP - chloroplast; L:D - light:dark cycle (unit: h: h); PFD - photon flux density (unit: $\mu\text{mol photons} \cdot \text{m}^{-2} \cdot \text{s}^{-1}$).

L:D	PFD	SW		CP		
		$^{12}\text{CO}_2$	$^{13}\text{CO}_2$	$R_{\text{PO}^{12}\text{C}}$	$R_{\text{PO}^{13}\text{C}}$	
24:0	15	33.4	0.372	19.3	0.212	
		30.1	0.334	17.7	0.193	
		19.0	0.211	17.7	0.194	
		19.7	0.219	18.0	0.198	
		13.1	0.145	17.4	0.191	
		27.0	0.300	39.8	0.436	
	30	23.0	0.256	34.6	0.379	
		18.4	0.205	31.3	0.342	
		16.7	0.186	33.6	0.367	
		11.8	0.131	27.5	0.301	
		28.9	0.321	83.6	0.915	
		27.0	0.300	68.1	0.745	
	80	19.3	0.215	64.6	0.706	
		19.1	0.212	56.9	0.622	
		11.6	0.129	52.1	0.569	
		29.7	0.330	65.9	0.720	
		22.4	0.249	58.5	0.640	
		17.7	0.197	69.8	0.763	
150	16.6	0.185	62.6	0.685		
	11.6	0.129	55.1	0.603		
	16:8	30	31.7	0.353	28.9	0.320
			23.5	0.262	27.8	0.307
			16.0	0.178	50.3	0.556
		80	10.8	0.120	37.8	0.418
5.2			0.058	30.4	0.335	
31.8			0.354	93.8	1.033	
23.9	0.266		104.7	1.153		
16.1	0.179		84.6	0.934		
12.4	0.138		81.2	0.894		
150	5.4	0.061	60.4	0.666		
	26.9	0.299	72.8	0.800		
	21.1	0.234	79.2	0.871		
	18.2	0.202	70.2	0.772		
	12.3	0.136	72.5	0.797		
	5.5	0.062	67.1	0.739		

covered by CO_2 diffusion only. Thus, external HCO_3^- has to be used as an additional carbon source which is well in line with the experimental findings of Rost et al. (2002); Bach et al. (2013), and Kottmeier et al..

Acknowledgements and funding information

We like to thank Dorothee Kottmeier, Sebastian Rokitta, and Björn Rost for many helpful discussions and comments on the manuscript. L.-M. H. was funded by the European Project on Ocean Acidification (EPOCA) and the Federal Ministry of Education and Research (BMBF, project: ZeBiCa²).

Appendix A

The four differential equations for the stable carbon isotope model depicted in Figure 4 read

$$\begin{cases} d[^{12}\text{CO}_2]^{\text{CS}}/dt \\ d[^{13}\text{CO}_2]^{\text{CS}}/dt \\ d[^{12}\text{CO}_2]^{\text{CP}}/dt \\ d[^{13}\text{CO}_2]^{\text{CP}}/dt \end{cases} = \begin{cases} R_{^{12}\text{CO}_2,\text{PM}}^{\text{CS}} - R_{^{12}\text{CO}_2,\text{CPm}}^{\text{CS}} \\ R_{^{13}\text{CO}_2,\text{PM}}^{\text{CS}} - R_{^{13}\text{CO}_2,\text{CPm}}^{\text{CS}} \\ R_{^{12}\text{CO}_2,\text{CPm}}^{\text{CP}} - R_{\text{PO}^{12}\text{C}}^{\text{CP}} \\ R_{^{13}\text{CO}_2,\text{CPm}}^{\text{CP}} - R_{\text{PO}^{13}\text{C}}^{\text{CP}} \end{cases} \quad (44)$$

where $[^{12}\text{CO}_2]^{\text{CS}}$ and $[^{13}\text{CO}_2]^{\text{CS}}$ stand for the concentrations of $^{12}\text{CO}_2$ and $^{13}\text{CO}_2$ inside the cytosol and $[^{12}\text{CO}_2]^{\text{CP}}$ and $[^{13}\text{CO}_2]^{\text{CP}}$ for the concentrations of $^{12}\text{CO}_2$ and $^{13}\text{CO}_2$ inside the bulk chloroplast.

$R_{^{12}\text{CO}_2,\text{PM}}^{\text{CS}}$ and $R_{^{13}\text{CO}_2,\text{PM}}^{\text{CS}}$ denote the rates by which the concentrations of $^{12}\text{CO}_2$ and $^{13}\text{CO}_2$ inside the cytosol change due to aquaporin-based diffusion across the plasma membrane. $R_{^{12}\text{CO}_2,\text{CPm}}^{\text{CP}}$ and $R_{^{13}\text{CO}_2,\text{CPm}}^{\text{CP}}$ give the corresponding rates for the bulk chloroplast.

$$R_{^{12}\text{CO}_2,\text{PM}}^{\text{CS}} = \gamma_{\text{CO}_2,\text{PM}} \cdot \frac{A^{\text{CS}}}{V^{\text{CS}}} \cdot ([^{12}\text{CO}_2]^{\text{SW}} - [^{12}\text{CO}_2]^{\text{CS}}) \quad (45)$$

$$R_{^{13}\text{CO}_2,\text{PM}}^{\text{CS}} = \gamma_{\text{CO}_2,\text{PM}} \cdot \frac{A^{\text{CS}}}{V^{\text{CS}}} \cdot ([^{13}\text{CO}_2]^{\text{SW}} - [^{13}\text{CO}_2]^{\text{CS}}) \quad (46)$$

$\gamma_{\text{CO}_2,\text{PM}}$ is the aquaporin-based permeability coefficient for CO_2 (Tab. 4) and $[^{12}\text{CO}_2]^{\text{SW}}$ and $[^{13}\text{CO}_2]^{\text{SW}}$ are given by Rost et al. (2002) (Tab. 8). A^{CS} and V^{CS} denote plasma membrane amount and cytosol volume, respectively (Tab. 3).

$$R_{^{12}\text{CO}_2,\text{CPm}}^{\text{CP}} = R_{^{12}\text{CO}_2,\text{PM}}^{\text{CS}} \cdot \frac{V^{\text{CS}}}{V^{\text{CP}}} \quad (47)$$

$$R_{^{13}\text{CO}_2,\text{CPm}}^{\text{CP}} = R_{^{13}\text{CO}_2,\text{PM}}^{\text{CS}} \cdot \frac{V^{\text{CS}}}{V^{\text{CP}}} \quad (48)$$

where V^{CP} (Tab. 3) gives the volume of the bulk chloroplast.

$R_{^{12}\text{CO}_2,\text{CPm}}^{\text{CP}}$ and $R_{^{13}\text{CO}_2,\text{CPm}}^{\text{CP}}$ indicate the rates by which the concentrations of $^{12}\text{CO}_2$ and $^{13}\text{CO}_2$ inside the bulk chloroplast change due to aquaporin-based diffusion across the chloroplast envelope. $R_{^{12}\text{CO}_2,\text{CPm}}^{\text{CS}}$ and $R_{^{13}\text{CO}_2,\text{CPm}}^{\text{CS}}$ give the corresponding rates for the cytosol.

$$R_{^{12}\text{CO}_2,\text{CPm}}^{\text{CP}} = \gamma_{\text{CO}_2,\text{CPm}} \cdot \frac{A^{\text{CP}}}{V^{\text{CP}}} \cdot ([^{12}\text{CO}_2]^{\text{CS}} - [^{12}\text{CO}_2]^{\text{CP}}) \quad (49)$$

$$R_{^{13}\text{CO}_2,\text{CPm}}^{\text{CP}} = \gamma_{\text{CO}_2,\text{CPm}} \cdot \frac{A^{\text{CP}}}{V^{\text{CP}}} \cdot ([^{13}\text{CO}_2]^{\text{CS}} - [^{13}\text{CO}_2]^{\text{CP}}) \quad (50)$$

$$R_{^{12}\text{CO}_2,\text{CPm}}^{\text{CS}} = R_{^{12}\text{CO}_2,\text{CPm}}^{\text{CP}} \cdot \frac{V^{\text{CP}}}{V^{\text{CS}}} \quad (51)$$

$$R_{^{13}\text{CO}_2,\text{CPm}}^{\text{CS}} = R_{^{13}\text{CO}_2,\text{CPm}}^{\text{CP}} \cdot \frac{V^{\text{CP}}}{V^{\text{CS}}} \quad (52)$$

$\gamma_{\text{CO}_2,\text{CPm}}$ gives the CO_2 permeability coefficient of the chloroplast envelope (Tab. 4). A^{CP} denotes the surface area of the chloroplast.

$R_{\text{PO}^{12}\text{C}}^{\text{CP}}$ and $R_{\text{PO}^{13}\text{C}}^{\text{CP}}$ give the fixation rates of $^{12}\text{CO}_2$ and $^{13}\text{CO}_2$ into PO^{12}C and PO^{13}C , respectively, that were calculated from the data of Rost et al. (2002).

References

- Anning, T., Nimer, M., Merrett, M.J., Brownlee, C., 1996. Costs and benefits of calcification in coccolithophorids. *Journal of Marine Systems* 9, 45–56.
- Bach, L.T., Riebesell, U., Schulz, K.G., 2013. Dissecting the impact of CO_2 and pH on the mechanisms of photosynthesis and calcification in the coccolithophore *Emiliania huxleyi*. *New Phytologist*, 1–14. <http://dx.doi.org/10.1111/nph.12225>.
- Berry, L., Taylor, A.R., Lucken, U., Ryan, K.P., Brownlee, C., 2002. Calcification and inorganic carbon acquisition in coccolithophores. *Functional Plant Biology* 29, 289–299.
- Billard, C., Inouye, I., 2004. What is new in coccolithophore biology? In: Thierstein, H.R., Young, J.R. (Eds.), *Coccolithophores - From molecular processes to global impact*. Springer, pp. 1–30.
- Boller, A., Phaedra, J., Cavanaugh, C., Scott, K., 2011. Low stable carbon isotope fractionation by coccolithophore *RubisCO*. *Geochimica et Cosmochimica Acta* 75, 7200–7207.
- Borkhsenius, O.N., Mason, C.B., Moroney, J.V., 1998. The intracellular localization of ribulose-1,5-bisphosphate Carboxylase/Oxygenase in *Chlamydomonas reinhardtii*. *Plant Physiology* 116 (4), 1585–1591.

- Brownlee, C., Davies, M., Nimer, N., Dong, L.F., Merrett, M.J., 1995. Calcification, photosynthesis and intracellular regulation in *Emiliana huxleyi*. *Bulletin de l'Institut océanographique océanographique* 14, 19–35.
- Herfort, L., Thake, B., Roberts, J., 2002. Acquisition and use of bicarbonate by *Emiliana huxleyi*. *New Phytologist* 156, 427–436.
- Holtz, L.-M., Thoms, S., Langer, G., Wolf-Gladrow, D.A., 2013. Substrate supply for calcite precipitation in *Emiliana huxleyi*: Assessment of different model approaches. *Journal of Phycology* 49, 417–426.
- Hopkinson, B.M., Dupont, C.L., Allen, A.E., Morel, F.M.M., 2011. Efficiency of the CO₂-concentrating mechanism of diatoms. *Proceedings of the National Academy of Sciences of the United States of America* 108 (10), 3830–3837.
- Kottmeier, D.M., Rokitta, S.D., Tortell, P.D., Rost, B., 2014. Strong shift from HCO₃⁻ to CO₂ uptake in *Emiliana huxleyi* with acidification: new approach unravels acclimation versus short-term pH effects. *Photosynthesis Research* 121 (2–3), 265–275.
- Mackinder, L., Wheeler, G., Schroeder, D., von Dassow, P., Riebesell, U., Brownlee, C., 2011. Expression of biomineralization-related ion transport genes in *Emiliana huxleyi*. *Environmental Microbiology* 13 (12), 3250–3265.
- NOAA, National Oceanic and Atmospheric Administration. Earth System Research Laboratory - Trends in Atmospheric Carbon Dioxide, (www.esrl.noaa.gov/gmd/ccgg/trends). Access: May 2013.
- Paasche, E., 1964. A tracer study of the inorganic carbon uptake during coccolith formation and photosynthesis in the coccolithophorid *Coccolithus huxleyi*, Scandinavian Society of Plant Physiology, Lund.
- Paasche, E., 2002. A review of the coccolithophorid *Emiliana huxleyi* (Prymnesiophyceae), with particular reference to growth, coccolith formation, and calcification-photosynthesis interactions. *Phycologia* 40 (6), 503–529, ISSN 0031-8884.
- Prasad, G.V.R., Coury, L.A., Finn, F., Zeidel, M.L., 1998. Reconstituted Aquaporin 1 water channels transport CO₂ across membranes. *The Journal of Biological Chemistry* 273 (50), 33123–33126.
- Pronina, N., Borodin, V., 1993. CO₂ stress and CO₂ concentration mechanism: investigation by means of photosystem-deficient and carbonic anhydrase-deficient mutants of *Chlamydomonas reinhardtii*. *Photosynthetica* 28, 515–522.
- Pronina, N., Semenenko, V., 1983. Localization of membrane-bound and soluble forms of carbonic anhydrase in the *Chlorella cell*. *Soviet Plant Physiology* 31, 241–251.
- Pronina, N., Semenenko, V., 1992. Role of the pyrenoid in concentration, generation and fixation of CO₂ in the chloroplast of microalgae. *Soviet Plant Physiology* 39, 470–476.
- Quiroga, O., González, E., 1993. Carbonic anhydrase in the chloroplast of a coccolithophorid (Prymnesiophyceae). *Journal of Phycology* 29, 321–324.
- Raven, J.A., 1997. CO₂-concentrating mechanisms: a direct role for thylakoid lumen acidification?. *Plant, Cell and Environment* 20, 147–154.
- Raven, J.A., Beardall, J., Giordano, M., 2014. Energy costs of carbon dioxide concentrating mechanisms in aquatic organisms. *Photosynthesis Research* 121, 111–124.
- Rokitta, S.D., Rost, B., 2012. Effects of CO₂ and their modulation by light in the life-cycle stages of the coccolithophore *Emiliana huxleyi*. *Limnology and Oceanography* 57 (2), 607–618.
- Rost, B., Zondervan, I., Riebesell, U., 2002. Light-dependent carbon isotope fractionation in the coccolithophorid *Emiliana huxleyi*. *Limnology and Oceanography* 47 (1), 120–128.
- Schulz, K.G., Rost, B., Burkhardt, S., Riebesell, U., Thoms, S., Wolf-Gladrow, D.A., 2007. The effect of iron availability on the regulation of inorganic carbon acquisition in the coccolithophore *Emiliana huxleyi* and the significance of cellular compartmentation for stable carbon isotope fractionation. *Geochimica et Cosmochimica Acta* 71, 5301–5312.
- Sültemeyer, D., Rinast, K.-A., 1996. The CO₂ permeability of the plasma membrane of *Chlamydomonas reinhardtii*: mass-spectrometric ¹⁸O-exchange measurements from ¹³C¹⁸O₂ in suspensions of carbonic anhydrase-loaded plasma-membrane vesicles. *Planta* 200, 358–368.
- Supuran, C.T., Scozzafava, A., 2007. Carbonic anhydrases as targets for medicinal chemistry. *Bioorganic & Medicinal Chemistry* 15, 4336–4350.
- Taylor, A.R., Chrachri, A., Wheeler, G., Goddard, H., Brownlee, C., 2011. A voltage-gated H⁺ channel underlying pH homeostasis in calcifying coccolithophores. *PLoS Biol* 9 (6), 1–13.
- Thoms, S., Pahlow, M., Wolf-Gladrow, D.A., 2001. Model of the carbon concentrating mechanism in chloroplasts of eukaryotic algae. *Journal of Theoretical Biology* 208, 295–313, ISSN 0022-5193.
- Uehlein, N., Otto, B., Hanson, D.T., Fischer, M., McDowell, N., Kaldenhoff, R., 2008. Function of *Nicotiana tabacum* aquaporins as chloroplast gas pores challenges the concept of membrane CO₂ permeability. *The Plant Cell* 20, 648–657.
- van der Wal, P., de Jong, E., Westbroek, P., de Bruijn, W., Mulder-Stapel, A., 1983. Ultrastructural polysaccharide localization in calcifying and naked cells of the coccolithophorid *Emiliana huxleyi*. *Protoplasma* 118, 157–168, ISSN 0033-183X.
- Vaughn, K.C., Campbell, E.O., Hasegawa, J., Owen, H.A., Renzaglia, K.S., 1990. The pyrenoid is the site of ribulose 1, 5-bisphosphate carboxylase/oxygenase accumulation in the hornwort (Bryophyta: Anthocerotae) chloroplast. *Protoplasma* 156, 117–129.
- von Dassow, P., Ogata, H., Probert, I., Wincker, P., Da Silva, C., Audic, S., Claverie, J.-M., de Vargas, C., 2009. Transcriptome analysis of functional differentiation between haploid and diploid cells of *Emiliana huxleyi*, a globally significant photosynthetic calcifying cell. *Genome Biology* 10, R114.1–R114.33.
- Wolf-Gladrow, D.A., Zeebe, R.E., Klaas, C., Körtzinger, A., Dickson, A.G., 2007. Total alkalinity: The explicit conservative expression and its application to biogeochemical processes. *Marine Chemistry*, 287–300.
- Zeebe, R.E., Wolf-Gladrow, D.A., 2001. CO₂ in seawater: equilibrium, kinetics, isotopes. Elsevier Science Ltd, Amsterdam, ISBN 0444505792.
- Zuddas, P., Mucci, A., 1994. Kinetics of calcite precipitation from seawater: I. A classical chemical kinetics description for strong electrolyte solutions. *Geochimica et Cosmochimica Acta* 58 (20), 4353–4362.